Summer 2023

Suppressing Aluminum/Silica Exchange Reaction Between High Aluminum Steel and Mold Flux During Continuous Casting Process

Kuanysh Nurbekuly Yermukhanbetov
Missouri University of Science and Technology

Department:

SUPPRESSING ALUMINUM/SILICA EXCHANGE REACTION BETWEEN HIGH ALUMINUM STEEL AND MOLD FLUX DURING CONTINUOUS CASTING PROCESS

by

KUANYSH NURBEKULY YERMUKHANBETOV

A THESIS

Presented to the Graduate Faculty of the

MISSOURI UNIVERSITY OF SCIENCE AND TECHNOLOGY

In Partial Fulfillment of the Requirements for the Degree

MASTER OF SCIENCE IN METALLURGICAL ENGINEERING

2023

Approved by:

Yijia Gu, Advisor
Ronald J. O'Malley, Co-advisor
Jeffrey Smith
Arezoo Emdadi

ABSTRACT

Mold flux plays one of the critical roles in continuous casting of steel. It performs five primary functions: thermal and chemical insulation, lubrication between the steel strand and mold, absorption of inclusions, and promotion of even heat flux. The aluminum/silica exchange reaction occurring between steel and mold flux during the continuous casting process poses significant challenges in the steel industry. This reaction can lead to various defects in the cast product and adversely affect its surface quality, as well as downstream processing.

In this work, effectiveness of two approaches, namely slag dopant additions and electrochemical techniques, in suppressing the exchange reaction between high aluminum steel and mold flux were investigated. Various slag dopants, including $CaSO_4$, $SrSO_4$, and SeS_2, were tested at concentrations of 0.5 wt.%, 1.0 wt.%, and 2.5 wt.%. The results demonstrated that all dopants tested slowed down the exchange reaction compared to the baseline condition. Among them, $SrSO_4$ and SeS_2 at a concentration of 0.5 wt.% exhibited slightly better suppression. However, increasing the dopant concentration above 1.0 wt.% did not further influence the reaction.

Moreover, the application of electrical potentials showed promising results in inhibiting the exchange reaction. Specifically, a voltage of 0.84 V and 1.0 V applied by steel electrode effectively suppressed the reaction, leading to increased aluminum content and decreased silicon content in the steel compared to the baseline condition.

ACKNOWLEDGMENTS

I would like to express my sincere gratitude to my advisors, Dr. O'Malley, and Dr. Gu, for their invaluable technical advice and guidance. I am also grateful to the Fulbright Program and the member companies of the Peaslee Steel Manufacturing Research Center (PSMRC) for providing funding for my education and this project. I extend my thanks to the industry members for their generous contribution of time, suggestions, and encouragement. I would like to specifically acknowledge Darrell Sturgill, Thinium Natarajan, and Joel Kohnke for their support throughout this project. I am grateful to Dr. Moats and Dr. Watts for their assistance in the research aspects, as well as my committee members Dr. Smith and Dr. Emdadi for their valuable time.

I am deeply indebted to Todd Sander for his expertise and continuous encouragement throughout all stages of this project. I would also like to express my appreciation to the entire MSE department, especially Teneke Hill, Emily Bullock, and Denise Eddings, for their support. My fellow graduate students, including Hanok Tekle, Hunter Parrish, and Tochukwu Princewill, have been always ready to make this journey more manageable, and I am grateful for their assistance.

I am incredibly thankful for the exceptional group of undergraduate students who contributed to this project. Nathan Gillespie, Matt Nosbush, Kris Phillips, and Christopher Rakers, thank you, I am truly grateful for your contributions. Lastly, I would like to express my heartfelt appreciation to my parents, relatives, and friends for their unwavering support, patience, and belief in me. They have been very supportive, keeping me motivated, maintaining my enthusiasm, and fostering a positive attitude throughout this endeavor.

TABLE OF CONTENTS

Page

LIST OF ILLUSTRATIONS

Figure Page

LIST OF TABLES

NOMENCLATURE

Symbol	Description
ΔG	Gibbs Free Energy Change
ΔH	Enthalpy Change
T	Temperature
ΔS	Entropy Change
K_{eq}	Equilibrium Constant
R	Gas Constant
n	Number of Electrons Involved in Reaction
F	Faraday's Constant
E	Electrical Potential
r	Rate of the Reaction
t	Time
k	Rate Constant
Θ	Surface Site
μ	Chemical Potential
μ_i^0	Standard Chemical Potential
a_i	Activity of the Element

1. INTRODUCTION

1. 1 OVERVIEW

The continuous casting process plays an important role in the production of high-quality steel, enabling the efficient and cost-effective transformation of liquid steel into solidified products. However, one of the major challenges faced during continuous casting of Al containing steel is the occurrence of the aluminum/silica exchange reaction between high aluminum steel and mold flux. This reaction, if uncontrolled, can lead to various detrimental effects such as surface defects, impaired product quality, and subsequent difficulties in downstream processing [1].

The aluminum/silica exchange reaction involves the diffusion of aluminum from the steel into the mold flux, while silicon diffuses from the mold flux into the steel. This interfacial reaction occurs due to the difference in chemical potential between aluminum and silicon in the steel and mold flux, respectively. The reaction not only affects the steel quality but also alters the composition and properties of the slag, which can further impact the casting process.

Suppression of the aluminum/silica exchange reaction is of importance to ensure the production of defect-free and high-quality steel. Various approaches have been explored to mitigate this reaction, and two promising techniques that have shown potential are slag dopant additions and electrochemical techniques.

Slag dopant additions involve the incorporation of specific elements or compounds into the mold flux to modify its chemical composition and properties. These additives can alter the thermodynamic and kinetic conditions at the steel-mold flux interface, thereby

reducing the possibility of aluminum and silicon exchange. Furthermore, electrochemical approach utilizes electromagnetic forces or electric currents to control the movement and distribution of the elements, minimizing the interfacial reaction between aluminum and silicon.

This thesis aims to investigate the effectiveness of slag dopant additions and electrical potential techniques in suppressing the aluminum/silica exchange reaction during the continuous casting process. By exploring these two approaches, we seek to provide valuable insights into their mechanisms of action and identify optimal strategies for minimizing the reaction.

1.2 ADVANCED HIGH STRENGTH STEELS

Advanced High Strength Steels (AHSS) with high aluminum content have emerged as a significant innovation in the automotive industry, providing remarkable opportunities for reducing the weight of vehicles and mitigating environmental emissions. These steels offer a combination of exceptional strength and reduced density, making them ideal for lightweighting applications.

By incorporating aluminum into the steel composition, AHSS achieves a remarkable reduction in weight without compromising structural integrity and safety. The addition of aluminum enhances the strength of the steel, allowing for the design of thinner, lighter components while maintaining or even improving their load-bearing capabilities. This weight reduction translates directly into improved fuel efficiency, as lighter vehicles require less energy to propel, resulting in reduced fuel consumption and lower greenhouse gas emissions. For instance, a decrease in weight by 10 kg over 200,000 km can result in

fuel consumption reduction of approximately 80 liters. For a vehicle weighing around 1500 kilograms, with steel accounting for 31% of its material composition, a weight saving of 30 kg achieved through aluminum rich AHSS would lead to a fuel consumption reduction of 240 liters. Extrapolating this impact over a year and accounting for the collective distance covered by millions of vehicles, the potential fuel savings and emission reductions become significant [2].

Additionally, the use of AHSS with high aluminum content contributes to a more sustainable future by reducing the reliance on fossil fuels. As the demand for lightweight materials grows, the need for energy-efficient transportation increases. Aluminum-rich AHSS enables the automotive industry to embrace cleaner and more efficient technologies, such as hybrid and electric vehicles. By reducing the weight of these vehicles, battery range can be extended, improving their overall efficiency, and reducing the need for frequent recharging.

Moreover, the advancements in manufacturing processes and material properties associated with AHSS with high aluminum content offer enhanced recyclability. Aluminum is highly recyclable, allowing for the recovery and reuse of this valuable material. The lifecycle analysis of vehicles made from aluminum-rich AHSS demonstrates a substantial reduction in energy consumption and emissions compared to traditional steel-intensive vehicles [2].

AHSS with high aluminum content have revolutionized the automotive industry by enabling the production of lightweight, yet strong and safe vehicles. Their positive impact on reducing weight and improving fuel efficiency leads to significant reductions in environmental emissions. With the ongoing pursuit of sustainability and environmental

stewardship, the adoption of aluminum rich AHSS represents a crucial step towards a greener and more sustainable future in the automotive sector.

1.3 EXCHANGE REACTION BETWEEN HIGH ALUMINUM STEEL AND MOLD FLUX

The production of Al containing AHSS through continuous casting presents certain challenges. A chemical reaction takes place between the Al in the steel and the SiO_2 present in the continuous casting flux. This reaction oxidizes the Al, converting it into Al_2O_3, and reduces the SiO_2 to Si. Consequently, Al_2O_3 replaces SiO_2 in the flux, while Si is introduced into the steel in place of Al. The chemical reaction and schematic are represented by Equation (1) and Figure 1.1 below [3].

$$3\,(SiO_2) + 4\,[Al] \leftrightarrow 3\,[Si] + 2\,(Al_2O_3) \quad (1)$$

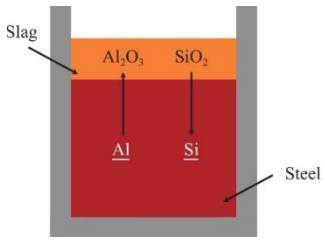

Figure 1.1 The Schematic Depicting the Mechanism of the Exchange Reaction.

This situation poses significant concerns as it results in wastage of the costly aluminum additions to the steel and alters the behavior of the flux due to the presence of Al_2O_3. These changes negatively impact the surface quality of the castings, leading to surface imperfections and, in severe cases, breakouts. Addressing these surface defects

before shipping the steel to customers incurs additional costs in terms of time and resources. Furthermore, breakouts pose substantial risks to the safety of the mill staff.

This project aims to mitigate the occurrence of the reaction between Al in the steel and Si in the flux by employing dopant additions and applying electrical voltage. The objective is to enable the safe and efficient production of high-Al steels with the most effective dopant concentration and electrical potential combination that would effectively prevent the reaction for an extended period.

1.4 CONTINUOUS CASTING PROCESS

In recent years, significant improvements have been made in the continuous casting process, leading to its widespread usage. Today, over 90% of global steel production relies on continuous casting [4]. In this highly efficient method, liquid steel is introduced into a water-cooled copper mold through a SEN, as depicted in Figure 1.2 [5]. It is at this stage that the solidification process initiates, giving rise to semifinished products such as slabs and billets, each possessing specific characteristics.

To shield the molten steel from oxidation, a layer of mold powder is applied atop the liquid steel within the mold. This powder melts and seeps into the space between the molten steel and the mold. The solidification of the steel shell and the management of heat transfer are regulated by the crystallization characteristics of the mold flux.

After leaving the mold, the steel strand undergoes a sequence of water sprays and support rollers as part of the continuous casting process. The water spraying action promotes effective heat transfer through the slab and enhances the cooling process. The

rate of solidification for each steel grade can be controlled by adjusting the water spray rate and the casting speed, allowing for tailored cooling conditions [6].

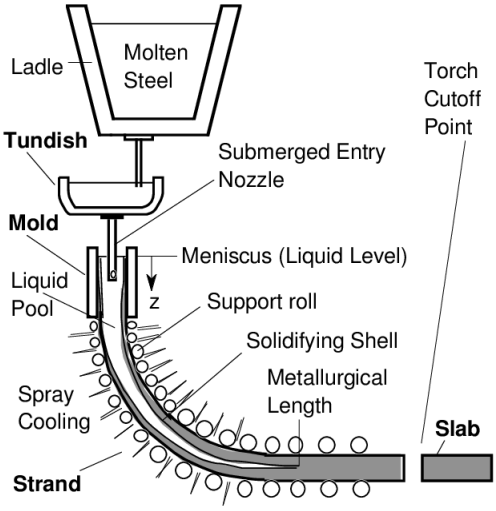

Figure 1.2 Schematic of Continuous Casting Process [7].

1.5 THE FUNCTIONS AND PROPERTIES OF MOLD FLUX

The mold fluxes are artificial slags composed of a complex combination of oxides, minerals, and carbonaceous materials. The primary oxides present include silica (SiO_2), calcium oxide (CaO), sodium oxide (Na_2O), aluminum oxide (Al_2O_3), and magnesium oxide (MgO). The ratios of (CaO/SiO_2) typically range from 0.7 to 1.3, with the addition of fluorite (F_2Ca) and carbonaceous materials incorporated into their compositions. The content levels of these compounds and their impact on the behavior of mold fluxes under process conditions are summarized in Table 1.1.

Table 1.1 Typical Composition of Mold Fluxes [8].

Characteristics	Compound	Amount in flux, wt. %
Glass formers	SiO_2	17 – 56
	Al_2O_3	0 – 13
	B_2O_3	0 – 19
	Fe_2O_3	0 – 6
Basic oxides or modifiers	CaO	22 – 45
	MgO	0 – 10
	BaO	0 – 10
	SrO	0 – 5
Alkalis	Na_2O	0 – 25
	Li_2O	0 – 5
	K_2O	0 – 2
Fluidizing	F	2 – 15
	MnO	0 – 5
Melting control	C	2 – 20

The utilization of mold fluxes throughout the continuous casting process plays a pivotal role in ensuring the attainment of desired product quality by performing various crucial functions such as thermal insulation, oxidation prevention, inclusion absorption, lubrication, and heat transfer. The last two functions are deemed crucial and require appropriate physicochemical characteristics of the mold powder, including viscosity,

crystallization behavior, fraction of crystalline slag film, interfacial tension, thermal properties of solid and liquid phases, etc. [9].

While the general effects of each component in the mold flux on its properties are understood, determining the optimal composition for a specific plant often involves a trial-and-error approach. A mold powder that works well in one plant may not yield the same performance in another plant due to variations in casting conditions, mold dimensions, steel grades, and operational differences between plants. Introducing a new steel grade typically requires the development of a new mold flux, which can be costly and time-consuming using this method. Therefore, in terms of this study, it is necessary to pay attention to the chemical composition of CaO-SiO_2 based mold fluxes, especially to the content of SiO_2 as its involved in exchange reaction between steel and mold flux.

The presence of SiO_2 is essential in conventional mold fluxes as it plays a vital role in controlling viscosity and influencing the crystallization properties of the molten slag by forming SiO_2 networks. However, when Al in molten steel reduces SiO_2, it significantly degrades the performance of the slag, which can disrupt the continuous casting process. Mold fluxes with lower SiO_2 contents can better tolerate the reactions between SiO_2 and Al since SiO_2 is not the primary functional component in such cases. However, when using a mold flux with low SiO_2 content, Na_2O plays a crucial role in regulating and stabilizing the performance of the flux. In this scenario, Al significantly reduces Na_2O. Therefore, the reduction of Na_2O during the casting process would negatively impact the stability and properties of the mold flux [10]. Thus, it can be stated that the properties and chemical composition of the mold flux have a significant impact on the exchange reaction between steel and mold flux, which has been studied by many researchers to this day.

1.6 CURRENT UNDERSTANDING ON ALUMINUM/SILICA EXCHANGE REACTION

The aluminum/silica exchange reaction between molten steel and flux during the continuous casting process has been a topic of significant research and understanding in the field of metallurgical engineering. This reaction plays a crucial role in the overall quality and cleanliness of the cast steel product. Studies have investigated the reaction mechanisms, composition evolutions, and microstructural changes at the steel-slag interface using various experimental techniques. The understanding of the aluminum/silica exchange reaction for optimizing the casting process and achieving improved steel quality will be discussed in this section.

Several decades ago, Stuart proposed a non-reactive mold flux system based on $CaO\text{-}Al_2O_3$, characterized by a high content of Al_2O_3 and a relatively low content of SiO_2. This design aimed to reduce the driving force of the slag/steel exchange reaction, making the resulting mold flux inert to Al in the molten steel. However, to meet the requirements of high-Al steel casting, fluxing agents needed to be added to adjust the properties of the $CaO\text{-}Al_2O_3$ slag system [11].

Then Cho et al. (2013) and Blazek et al. (2011) developed $CaO\text{-}Al_2O_3$-based mold fluxes and conducted cast trials. When the CaO/Al_2O_3 ratio of the mold flux was 1, the results indicated a significant reduction in the slag/steel exchange reaction and an obvious improvement in the surface quality of cast slabs. However, this led to poor mold flux consumption and lubrication properties, resulting in drag marks on the slab surface. Consequently, these mold fluxes were not beneficial for the continuous casting process [12,13]. J. Yang et al. (2019) also investigated the reaction between high-Al steel and $CaO\text{-}Al_2O_3$-based mold fluxes with varying CaO/Al_2O_3 ratios at 1773 K (1500 °C). They found

that increasing the CaO/Al_2O_3 ratio promoted the accumulation of Al_2O_3 in the flux and no effect on the reduction of SiO_2 [14].

S. Song et al. (2022) and Y. Kang et al. (2012) conducted experiments to examine the reactions between high aluminum steel and a $CaO\text{-}SiO_2$ based mold flux. They identified that the metal-slag reaction reached a stable state after about 10 minutes where the rate-controlling step in the reaction was the mass transfer of Al in the molten steel [15,16].

In addition, the laboratory experiments with different MgO content by M. Kim et al. (2012, 2018) revealed that Al_2O_3 quickly accumulated near the flux interface, while reductions in SiO_2 and Na_2O occurred regardless of the initial MgO content. Solid phases such as magnesium aluminate ($MgAl_2O_4$), calcium aluminate ($CaAl_4O_7$), and additional Al_2O_3 were observed due to local MgO depletion in the flux. Also, factors such as (pct CaO/pct SiO_2), (pct Al_2O_3), [pct Al], [pct Si], and temperature were varied to determine their influence on the reaction. The results indicated that the reaction was primarily governed by the Al content in the molten steel, while temperature had a minor effect [17,18].

H. Yu et al. (2022) examined the influence of varying aluminum content on the changes in composition of steel and slag, in high-Mn-high-Al steel when exposed to $CaO\text{-}SiO_2\text{-}Al_2O_3\text{-}MgO$ slag. They observed that as the initial Al content increased, Al gradually replaced Mn in reacting with SiO_2 in the slag to prevent manganese loss [3].

Also, He et al. (2009) found that the introduction of MnO can prevent significant reduction of SiO_2 in the slag. This is because when the MnO content surpasses a specific threshold, it becomes more favorable for SiO_2 to react with Al [19]. However, Blazek et

al. (2011) proposed that an increase in the MnO content would lead to a more active interaction between slag and steel, as evidenced by monitoring the real-time chemical changes in the mold slag [20].

Wang et al. (2012) additionally created a mathematical model for kinetic calculations to predict the variation of Al_2O_3 in the molten slag during the continuous casting process of high-Al steel. According to their findings, the concentration of Al_2O_3 in the mold slag experienced rapid growth in the early phase, and this change was primarily influenced by the initial concentration of Al_2O_3 [21].

Furthermore, Ozturk and Turkdogan (1984) suggested that when the SiO_2 content in the mold flux varies from 5 to 10 wt.%, the reaction between the slag and steel can be hindered because of the considerable decrease in SiO_2 activity [22]. A Japanese patent [23] also demonstrated similar findings, indicating that if the SiO_2 content is less than 7 wt.%, the reaction between SiO_2 in the mold flux and Al in the molten steel would not occur significantly.

Different kinetic and thermodynamic models were developed by Y. Kang et al. (2012) and M.-S. Kim et al. (2016) to predict the accumulation of Al_2O_3, SiO_2 and the rate-controlling steps. These models considered factors such as temperature, initial alloy composition, and flux viscosity. The results obtained from the models aligned well with experimental data and provided a deeper understanding of the reaction mechanisms [16,24].

Various studies have explored the mechanisms, composition changes, and microstructural alterations at the steel-slag interface during the aluminum/silica exchange reaction using different mathematical models, compositions of steel and mold flux,

temperatures, etc. However, the aluminum/silica exchange reaction still require more investigations to be done, especially understanding of its kinetic and thermodynamic states, which will be discussed further.

2. METHODOLOGY

The aluminum/silica exchange reaction between steel and mold flux during continuous casting involves both thermodynamics and kinetics. Thermodynamically, the driving force for the reaction is the difference in chemical potentials between the products (Al_2O_3 and Si) and the reactants (Al in the steel and SiO_2 in the flux). Kinetically, the rate at which the aluminum/silica exchange reaction occurs is influenced by several factors such as temperature, steel and mold flux composition, area of the reaction interface, the diffusion of the reacting species, etc.

Understanding the thermodynamics and kinetics of the aluminum/silica exchange reaction is essential for optimizing the continuous casting process. By studying these aspects, researchers can gain insights into the factors influencing the reaction rate, develop strategies to control or optimize the process, and improve the quality of the cast products.

2.1 REACTION THERMODYNAMICS

Thermodynamic analysis plays a crucial role in obtaining the fundamental principles underlying this exchange reaction. The primary objective is to determine the conditions under which the reaction can be controlled or suppressed. The driving force for the reaction is the difference in chemical potentials between the reactants and products of the exchange reaction.

The equilibrium state of the aluminum/silica exchange reaction can be analyzed using thermodynamic calculations, which involve the determination of the Gibbs free

energy change (ΔG) associated with the reaction. The Gibbs free energy change and equilibrium constant can be calculated using the Equation (2) and Equation (3):

$$\Delta G° = \Delta H° - T\Delta S°, [J] \quad (2)$$

$$K_{eq} = e^{-\Delta G /RT} \quad (3)$$

where ΔH° is the enthalpy change, ΔS° is the entropy change of the reaction, T is a temperature, K_{eq} is the equilibrium constant, and R is the gas constant. The following data of the exchange reaction at temperature of 1600 ℃ with pure compounds were obtained by calculations: ΔG° = -421.9 kJ, ΔH° = -527.6 kJ, ΔS° = -56.4 J, $K_{eq} = 5.8 \cdot 10^{11}$.

Additionally, electrical potential was calculated for the reaction with pure compounds using the following Equation 4:

$$\Delta G° = -nFE, [J] \quad (4)$$

where, n is the number of electrons involved in the reaction, F is the Faraday's constant, E is the electrical potential. The value of electrical voltage calculated using Equation (4) turned out to be 0.36 volts.

This change in free energy provides valuable information about the feasibility and direction of the reaction. By comparing the thermodynamic equilibrium conditions with the actual operating conditions in the continuous casting process, it is possible to gain insights into the kinetics and mechanisms of the reaction. For instance, thermodynamic

analysis helps in identifying the factors that influence the rate of the exchange reaction. Parameters such as temperature, composition of the steel and flux, and the presence of impurities can significantly impact the thermodynamic properties and subsequently affect the reaction kinetics [18].

Overall, it should be concluded that any changes in experimental parameters such as temperature or chemical compositions of steel and mold flux will affect the activities and chemical potentials of important species in solutions, especially with the electrochemical approach where the critical electrical potential needed to suppress the exchange reaction will be directly related to those factors.

2.2 REACTION KINETICS

The kinetics of the aluminum/silica exchange reaction between high aluminum steel and mold flux during continuous casting involve understanding the rate at which the reaction occurs and the factors that influence its progress. The reaction typically involves the exchange of aluminum Al from the steel with silica SiO_2 in the mold flux, leading to the formation of aluminum oxide Al_2O_3 in the flux and the incorporation of silicon Si into the steel, which can be seen in Equation (5).

The rate at which exchange reaction occurs can be written in the following form:

$$r = -\frac{1}{4}\frac{d[Al]}{dt} = -\frac{1}{3}\frac{d[SiO2]}{dt} = \frac{1}{3}\frac{d[Si]}{dt} = \frac{1}{2}\frac{d[Al2O3]}{dt} = k\,[Al]^m[SiO_2]^n \qquad (5)$$

where, r is the rate of the reaction, *t* is the unit of time, k is the rate constant, [Al], [Si], [Al_2O_3] and [SiO_2] are the initial concentrations of reactants and products, m and n values depend on the experimental report of kinetics data.

Based on the reaction rate described above, one can easily find the factors influencing the kinetics of this reaction:

1. Temperature: The reaction rate generally increases with temperature, as higher temperatures provide greater thermal energy for the diffusion of aluminum and silicon ions across the steel-flux interface. Elevated temperatures also enhance the reactivity of the materials involved.

2. Alloy composition: The aluminum content in the high aluminum steel plays a crucial role in the kinetics of the reaction. Higher aluminum concentrations in the steel lead to more rapid aluminum/silica exchange due to increased availability of aluminum atoms for the reaction.

3. Mold flux composition: The composition of the mold flux, particularly the amount of silica (SiO_2), can influence the kinetics of the reaction. A higher SiO_2 concentration in the flux provides more reactants for the aluminum/silica exchange reaction and can lead to faster reaction rates.

4. Reaction interface: The area and nature of the steel-flux interface also affect the kinetics of the reaction. A larger interfacial area facilitates a higher rate of exchange, while factors such as surface roughness or the presence of oxide films can hinder the reaction kinetics.

5. Mass transfer: The transport of aluminum and silicon species across the steel-flux interface is a key step in the kinetics of the reaction. Mass transfer mechanisms, such

as diffusion or convective flow, determine the rate at which the reactants can interact and participate in the exchange reaction.

In general, the rate of the overall reaction between molten steel and molten flux is controlled by three steps: mass transfer in the molten steel phase, chemical reaction(s) at the interface, and mass transfer in the molten flux phase. This study considering only the kinetics at the interface between liquid steel and molten flux phases. Reaction (1) can be divided into several elementary steps, including:

1. Mass transfer of Al and SiO_2 from bulk to the interface in their respective phases.
2. Mass transfer of Si from the interface to bulk in the molten steel.
3. Mass transfer of Al_2O_3 from the interface to bulk in the molten flux.
4. Chemical reaction - breaking of the Si-O bond of SiO_2 at the interface.
5. Formation of the Al-O bond of Al_2O_3 at the interface.

Among these steps, Step 4 and Step 5 involve chemical reactions. Step 4 is expected to be temperature-dependent due to the high activation energy required, while Step 5, involving the formation of the Al-O bond, is less likely to control the overall reaction rate due to the strong affinity between Al and O. However, if Step 4 is slow, similar to the reduction of SiO_2 by C, the overall reaction rate in this case could be significantly influenced by temperature. Y-B. Kang et al. (2012) have shown that the rate of Al_2O_3 accumulation is affected by temperature, although the extent of the effect is not described as "significant"[16].

The Langmuir kinetics model assumes that the exchange reaction rate is proportional to the concentration of the surface-active species in the bulk phase and the number of vacant adsorption sites on the surface. Therefore, Langmuir surface reaction

kinetics model was employed to analyze the behavior at the interface's slag side. It is assumed that activities of species in solution increase during the occupation of surface-active sites. The subsequent equations were derived using $SrSO_4$ slag dopant as an illustrative case.

$$SiO_2 + \square \rightleftharpoons SiO_2^* \quad (1 - \text{equilibrium}) \tag{6}$$

$$SiO_2^* \rightarrow \underline{Si} + 2\underline{O} \qquad (2 - \text{slow}) \tag{7}$$

$$SrSO_4 + \square \rightleftharpoons SrSO_4^* \ (3 - \text{equilibrium} - \text{surface active}) \tag{8}$$

$$2\underline{Al} + 3\underline{O} \rightarrow Al_2O_3^* \ (\text{fast}) \tag{9}$$

$$Al_2O_3^* \rightarrow Al_2O_3 + \square \ (\text{fast}) \tag{10}$$

$$k_1 = \frac{a_{SiO_2} * \square}{\Theta_{SiO_2}} \tag{11}$$

$$r_{SiO2} = k\,\Theta_{SiO2} \tag{12}$$

$$\Theta_{SiO2} = \frac{k_1\, a_{SiO2}}{1 + k_1\, a_{SiO2} + k_3\, a_{SrSO4}} \tag{13}$$

where, Θ_{SiO2} is the surface sites occupied by SiO_2, Θ_{SrSO4} is the surface sites occupied by $SrSO_4$, r is the rate of the reaction and k is the rate constant [25].

Understanding the kinetics of the aluminum/silica exchange reaction is crucial for optimizing the continuous casting process. Experimental techniques, such as in-situ observations, thermodynamic modeling, and mathematical modeling, are commonly employed to study the reaction kinetics and elucidate the underlying mechanisms. By investigating these factors, researchers can gain insights into the kinetics of the aluminum/silica exchange reaction and develop strategies to control or optimize the process during continuous casting.

In this study, we explore two methods to suppress the aluminum/silica exchange reaction. The first method explores the possibility to suppress the reaction by blocking the surface sites using dopant additions (Section 3). The second method explores the possibility of controlling the exchange reaction by applying external electrical voltage to reduce the driving force (Section 4).

3. SLAG DOPANTS ADDITION

Surface active species are molecules that possess unique properties at the interface between two different phases, leading to preferentially locate themselves at the metal-slag interface and reduce the surface tension between two phases, allowing them to mix or spread more easily. For instance, SeS_2 slag dopant consists of sulfur, which is a strong surface-active agent, it occupies the surface-active sites in molten steel, while selenium reacts with compounds in molten flux. The objective of slag dopant addition is to prevent the occurrence of the exchange reaction at the interface between the liquid flux and the molten steel. In theory, this should establish a barrier between the two regions, effectively inhibiting the reaction from taking place.

The purpose of this approach was to conduct laboratory tests to examine the effectiveness of slag dopants, based on previous investigations, namely $SrSO_4$, $CaSO_4$, and SeS_2, in suppressing the aluminum/silica exchange reaction. The simple mechanism on how dopant additions block surface active sites is illustrated in Figure 3.1. The concentrations of these dopants ranged from 0 to 2.5 wt. %. By investigating the impact of these specific dopants, it was planned to gain insights into their potential as additives for controlling and mitigating the undesired reaction at the steel-slag interface. The findings from these tests provide valuable information for enhancing the knowledge of suppressing the aluminum/silica exchange reaction, leading to improved continuous casting process and better steel quality.

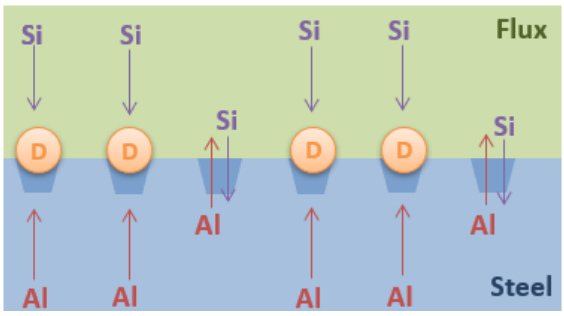

Figure 3.1 A Diagram Showing How the Dopants Block Exchange Reaction by Occupying Surface Active Sites.

3.1 MATERIALS AND METHODS

The steel employed in the experimental study was manufactured internally and its composition was determined using Optical Emission Spectroscopy (OES), with the results presented in Table 3.1. The flux utilized in the study was obtained from Imerys Metalcasting Solutions and its composition, as reported by Imerys, along with measurements obtained after the processing steps described later, are listed in Table 3.2. X-ray Fluorescence (XRF) analysis was employed to obtain both sets of measurements. Additionally, three dopants were incorporated into the flux: $CaSO_4$ obtained from Arcos Organics with a purity of 98%, $SrSO_4$ with a purity of 99.5%, and Se_2S with a purity of 97% both purchased from Alfa Aesar.

Table 3.1 The Starting Composition of the Steel, Measured by OES.

Element	Fe	C	Si	Al
Wt%	Bal.	0.12	0.48	2.84

Table 3.2 The Staring Composition for the Flux, Measured by XRF.

Component	As received (wt.%)	Processed (wt.%)
SiO_2	32.0	37.5
CaO	30.4	35.2
MgO	3.1	3.5
Al_2O_3	4.1	4.7
Fe_2O_3	0.2	0.3
Na_2O	8.7	9.9
F	7.9	11.3

The initial step of the procedure involved the preparation of the flux. Upon receipt, the base flux underwent a calcination process to eliminate impurities. The calcining procedure consisted of gradually heating the flux from room temperature to 725 ℃ at a rate of 5 ℃/min, holding it at 725 °C for a duration of 5 hours, and subsequently cooling it back to room temperature at the same rate. Calcined and as-received mold fluxes are shown in Figure 3.2.

(a) (b)

Figure 3.2 As-received (a) and Calcined (b) Mold Flux.

Then, precise quantities of the calcined base flux and dopants were measured and combined to achieve the desired dopant weight percentage of either 0.5, 1.0 or 2.5 wt.%. The resulting mixture of flux and dopant was then placed in a furnace and heated to a temperature of 1300 °C to facilitate melting. The mixture remained in the furnace until complete melting was observed, which typically occurred within approximately 5-6 minutes. Following this, the mixture was promptly removed from the furnace and rapidly quenched into a glass material before being broken and collected. The resulting glass material was subsequently finely ground in preparation for the experimental trials.

(a) (b)

Figure 3.3 Pictures of Melted (a) and Quenched (b) Glass Material.

For the experimental tests, a batch of steel was cast and sectioned to attain an approximate weight of 80 and 160 grams. Prior to commencing the trials, the steel material underwent polishing procedures to ensure the absence of any additional oxides.

3.2 EXPERIMENTAL SETUP

The experiments were performed in two muffle furnaces which are shown in Figure 3.4 along with magnesia (MgO) crucible, glass, and steel sample.

(a) (b)

Figure 3.4 Muffle Furnaces (a), MgO Crucible, Glass, and Steel Sample (b) Used in Experiments.

The high density MgO crucibles had an internal diameter of 35 mm and height of 87 mm. This size allowed the placement of 6-8 crucibles inside the furnace in each test with maximum productivity. Two alumina plates were placed in furnaces to protect the samples and interior of the furnaces. The steel and glass masses varied between 80-160 g and 30-60 g respectively with the same steel/slag proportion. The experimental configuration of crucible and its arrangement in the furnace is shown in Figure 3.5.

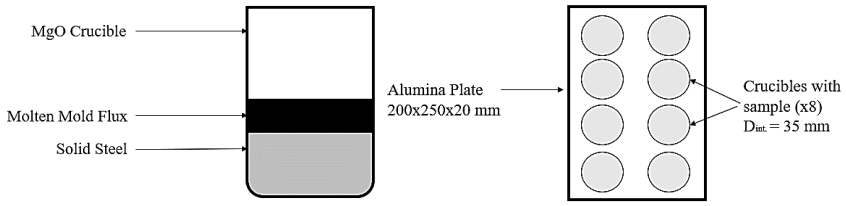

(a) (b)

Figure 3.5 Experimental Configuration of (a) Crucible and (b) Its Arrangement in the Furnace.

3.3 DETERMINATION OF THE MELTING POINT OF STEEL

To ensure the accuracy of the experiments, it was important to ascertain the steel's melting point, which refers to the time required for the sample to completely liquefy at a temperature of 1600℃. To achieve this, a 300 mm long alumina rod was affixed to the steel sample beforehand and placed within a MgO crucible in the furnace. The furnace was then gradually heated to 1600℃, with the MgO crucible inside, to prevent any abrupt thermal changes. Then steel sample was preheated for 5 minutes at 1400℃ in another muffle furnace once the temperature in first furnace reached 1600℃. The hot steel sample was then placed in already preheated MgO crucible and put in the furnace with the temperature 1600℃. Periodic assessments of the steel sample's state of aggregation were conducted by inserting an alumina rod through an aperture in the furnace cover. As a result, the following melting times were determined: 8 minutes for a 160-gram steel sample and 7 minutes for an 80-gram steel sample. The arrangement of the trial is shown in Figure 3.6.

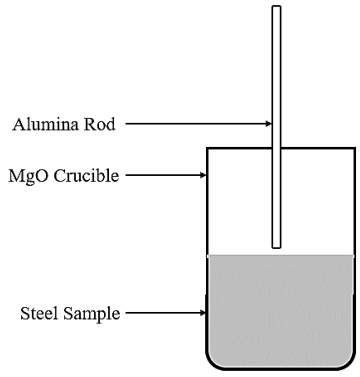

Figure 3.6 The Arrangement of Alumina Rod Inside the MgO Crucible.

3.4 EXPERIMENTAL PROCEDURE

During the experimental procedure, two furnaces were activated and brought up to the desired temperatures of 1600 and 1400 ℃. Prior to heating, up to eight MgO crucibles were carefully positioned inside the furnace operating at 1600°C to undergo preheating. This precautionary measure aimed to minimize the likelihood of thermal shock-induced cracking in the crucibles. Simultaneously, an Al_2O_3 crucible was introduced into the second furnace for the same purpose.

Once both furnaces reached the desired temperature, a graphite crucible containing the flux material was placed inside the 1400°C furnace to facilitate its melting. Subsequently, a steel sample was inserted into the same furnace and allowed to preheat for a duration of five minutes as a preliminary step. Following the preheating process, the steel sample was transferred to one of the preheated MgO crucibles in the 1600°C furnace. This transfer ensured that the steel would not cool down while the molten flux was retrieved from the other furnace.

The molten flux was carefully poured over the steel sample, after which the crucible containing the steel and flux was returned to the 1600℃ furnace to undergo a designated period of rest. The duration of this rest period varied depending on the specific trial and could last for fifteen minutes. The initial seven or eight minutes (depending on the weight of steel sample) of the rest period allowed the steel to achieve complete molten state, while the remaining time constituted the actual duration of the reaction.

Upon removal from the furnace, the steel sample underwent quenching in water media, followed by subsequent separation of the flux from the steel. Optical Emission Spectroscopy (OES) analysis was then conducted on the steel sample, while the flux was

sent for X-ray Fluorescence (XRF) analysis. The combined results of these analyses provided insights into the extent of the expected exchange reaction that typically takes place between the steel and the flux.

3.5 RESULTS AND DISCUSSION

Each slag dopant employed exhibited an impact on the exchange reaction occurring between the silicon present in the flux and the aluminum contained within the steel. This is proven by a comparative analysis of the reaction involving the base flux and the reaction involving any of the doped fluxes, as depicted in Figure 3.7 and Figure 3.8. Over an extended period, the base flux demonstrates a progressive accumulation in the silicon content of the steel; however, the rate of the reaction gradually decreases as it approaches its completion. This decline signifies a retention of aluminum within the steel, thereby showing the intended functionality of the dopants.

When all three dopants are utilized, increase in the dopant quantity does not impact the exchange reaction. The content of Si in the steel remains constant as the dopant amount increases. Depending on the observed data point, either 1.0 wt.% or 2.5 wt.% results in a lower Si content in the steel.

Specifically, in the case of SrSO4, each data point at 2.5 wt.% exhibits a higher Si content compared to the 1.0 wt.% data point. This indicates that these data points fall within the margin of error, and one cannot be considered better than the other. Based on these findings, it can be inferred that the flux has reached a state of saturation with the dopant. Therefore, the future tests required lowering the amount of dopant content in the flux.

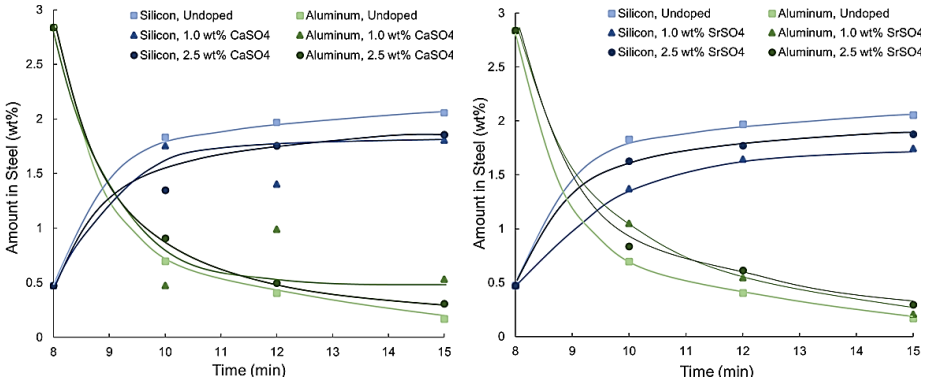

(a) (b)

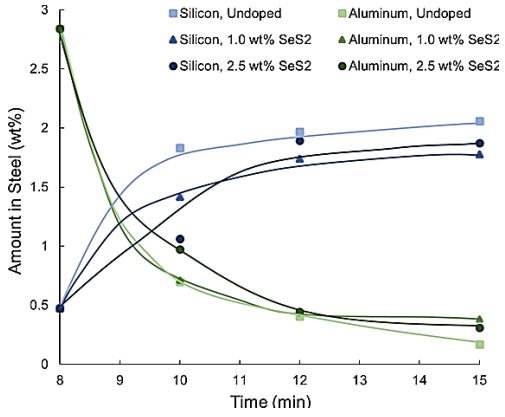

(c)

Figure 3.7 OES Analysis of Steel Samples With (a) $CaSO_4$, (b) $SrSO_4$ and (c) SeS_2 Dopant Additions Compared to Baseline With 160/60 g Steel/Slag Ratio.

The experiments with 1.0 wt.% and 2.5 wt.% of slag dopants were performed employing 160 g of steel combined with 60 g of flux. Throughout the testing process, cases were observed where the molten slag expelled from the MgO crucible within the furnace.

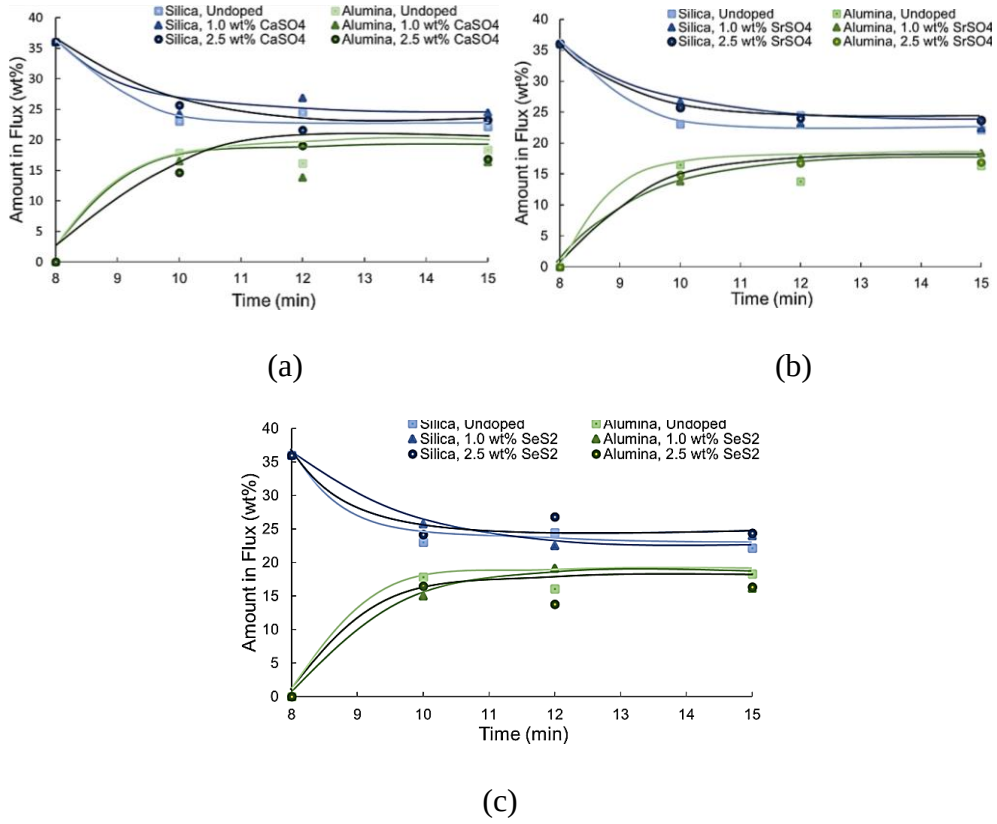

Figure 3.8 XRF Analysis of Slag Samples With (a) $CaSO_4$, (b) $SrSO_4$ and (c) SeS_2 Dopant Additions Compared to Baseline With 160/60 g Steel/Slag Ratio.

Consequently, a decision was made to reduce the amounts of both steel and slag while maintaining the same proportion, resulting in a revised ratio of 80 g of steel and 30 g of flux. The reduced amount was used to conduct experiments with lower dopant concentrations of 0.5 wt.% and additionally 1wt.% to confirm previous results. Results of the OES and XRF analysis are shown in Figure 3.9 and Figure 3.10.

It is observed that the addition of $CaSO_4$ to the slag did not exhibit significant suppression of the exchange reaction when compared to the baseline at both concentrations.

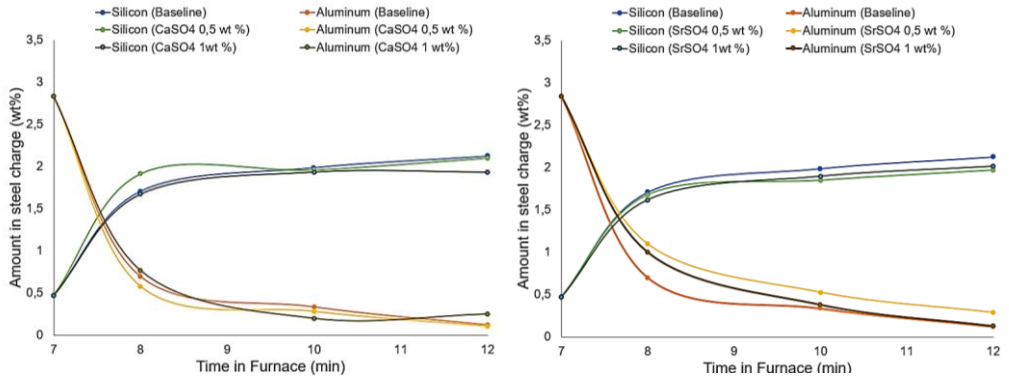

(a) (b)

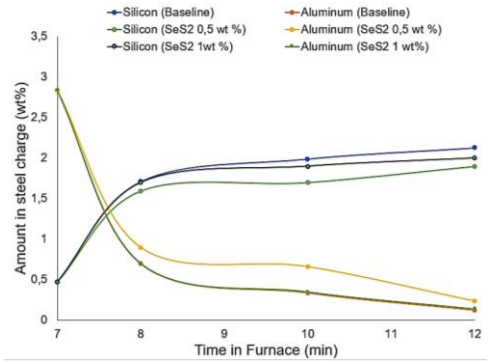

(c)

Figure 3.9 OES Analysis of Steel Samples with (a) $CaSO_4$, (b) $SrSO_4$ And (c) SeS_2 Dopant Additions Compared to Baseline with 80/30 g Steel/Slag Ratio.

Conversely, the inclusion of $SrSO_4$ and SeS_2 dopants in the slags at a concentration of 0.5 wt.% demonstrated a slightly improved suppression of the exchange reaction, resulting in higher Al content and lower Si content in the steel compared to the baseline. This effect was particularly notable in the case of SeS_2 dopant addition. Furthermore, it is worth noting that the suppression of the reaction is clear during the initial 3-minute period, after which the reaction proceeds to completion. Detailed XRF results of all slag samples can be seen below.

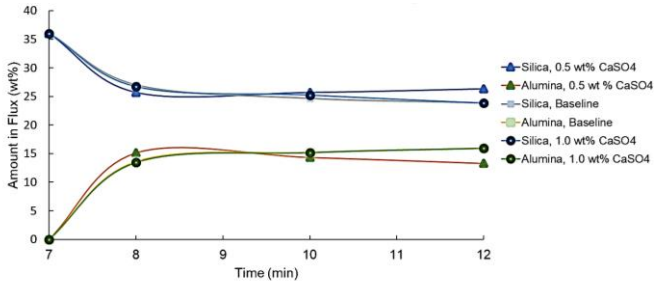

(a)

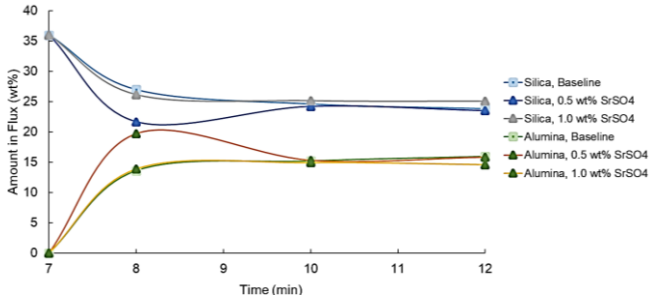

(b)

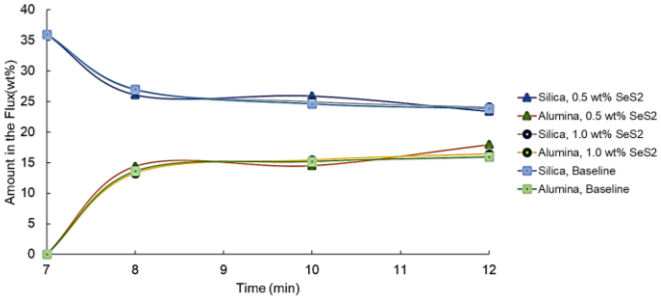

(c)

Figure 3.10 XRF Analysis of Slag Samples with (a) $CaSO_4$, (b) $SrSO_4$ and (c) SeS_2 Dopant Additions Compared to Baseline with 80/30 g Steel/Slag Ratio.

During the analysis of XRF and OES data, only the OES data utilizing the Si content in the steel was utilized for drawing conclusions. While conducting the experiment, it was observed through XRF analysis that the slag exhibited an increase in MgO and Na_2O

content from 3.5 to 12.0 wt.% and 9.9 to 8.0 wt.% respectively. This phenomenon was attributed to the degradation of the MgO crucibles during the experiment, leading to the release of MgO into the slag and potential reduction of Na_2O by Al in steel. Such an occurrence introduces an unexplained content change of other elements present in the slag when weight percentages are considered.

Furthermore, the presence of Al in the steel can be influenced by variations in process times during the experiment, thereby yielding unreliable measurements. Referring to the Ellingham diagram, it is established that Al_2O_3 is thermodynamically more stable than Si. Consequently, the oxidation of Al is favored over Si in this reaction. Based on this information, it can be inferred that Si's reaction takes place between the steel and the flux, thereby making it the most reliable parameter for analysis.

To estimate the potential error in the optical emission spectroscopy (OES) data, a mass balance analysis was conducted. Prior to the experiments, the steel and flux were weighed, and subsequently, the steel was weighed again after the experiments. However, due to the flux adhering to the MgO crucible during the quenching process, its weight was not measured. Instead, an assumption was made that the quantity of CaO in the flux remained constant. By utilizing the change in weight percentage (wt.%) of CaO, a determination was made for the weight of the flux following the experiment.

Since CaO is considered a more stable oxide compared to Al_2O_3, it was anticipated that its interaction with the steel would differ from that of SiO_2. By combining these weights with the known compositions of the steel and flux, both before and after the experiments, as determined through OES and XRF techniques, it became possible to monitor the progression of the reaction within the steel. By comparing the variation in the

amount of Al in the steel with the amount predicted by Equation (1), it was feasible to assess the extent of Al that reacted with SiO_2 in the flux and the portion that underwent oxidation with the air.

If aluminum in steel is not properly protected from oxidation during experiments, it can be consumed through a reaction with oxygen in the atmosphere. Aluminum is highly reactive and readily forms aluminum oxide (Al_2O_3) when exposed to oxygen due to its high chemical affinity. This oxidation reaction reduces the aluminum content in the steel. The presence of mold flux can potentially provide a protective layer on the surface of the steel, preventing direct contact between the molten steel and the surrounding atmosphere. However, if the mold flux is not effective in creating a sufficient barrier, or if there are defects or cracks in the mold flux layer, oxygen can still penetrate and react with the aluminum in the steel.

Since Al can undergo reactions with the air, it is unreliable for predicting the disparity between the values predicted by Equation (1) and the actual redox reaction occurring between the flux and the steel in an experimental setting. Hence, a more reliable approach for quantifying the experimental error entailed tracking the changes in the amount of Si in the steel and comparing it with the predictions made by Equation (1).

The Al oxidation levels displayed in Table 3.3 demonstrate a doubling in the proportion of Al reacting with air when comparing experiments using undoped fluxes to those employing doped fluxes. Given that the same experimental procedure was followed for all cases, it is unlikely that the amount of Al reacting with air varies significantly between experiments.

Table 3.3 The Amount of Al Reacted with Air Instead of the Flux, Calculated in the Mass Balance.

Reaction Type	Average Percent of Total Al Reacted with Air
Undoped fluxes	30%
Doped fluxes	60%
All experiments	45%

Instead, it is more plausible that there is a reduced amount of Al reacting with SiO_2 in the flux, causing the proportion of Al reacting with air to constitute a larger portion of the total Al loss in the steel. This observation aligns with the outcomes of the OES analysis, which indicated higher Al content in the steels subjected to experiments with doped fluxes. Hence, the dopants function as postulated, effectively preventing the Al-Si exchange between the steel and flux.

Upon comparing the measured Si gain in the steel with the Si amount predicted by Equation (1), an average deviation of 10% was observed across all experiments. This discrepancy can potentially be attributed to two factors. Firstly, the glassy flux might have experienced popping out of the crucible during the melting process due to residual stresses. Secondly, there could have been inadequate mixing of the dopant into the flux during the glass formation stage, resulting in the actual fluxes used in the experiments deviating from the intended composition. For instance, when transferring the flux into the graphite crucible for melting, a weight boat was employed, and this process occasionally left small amounts of flux in the weight boat. If the dopant was not thoroughly mixed with the flux, the weight boat could primarily consist of dopant, leading to a lower dopant content in the produced

flux. Nevertheless, despite these factors, the discrepancy in the initial and final Al and Si contents for the steel exceeds 10%, confirming that a reaction between the flux and steel indeed took place. Furthermore, when comparing the Al and Si contents of the doped reactions with the undoped reaction, the differences also surpass 10%, signifying that the dopants effectively inhibited the exchange reaction, and the disparity in values is not solely due to experimental variability.

3.6 SUMMARY

The effect of dopant additions on the exchange reaction between a high aluminum steel and mold flux was studied for the continuous casting process. Slag dopants with surface-active species obtained from $CaSO_4$, $SrSO_4$ and SeS_2 additions were chosen to suppress the aluminum/silica exchange reaction. Experimental data shows that all dopants with compositions of 0.5, 1.0 and 2.5 wt.% slowed the rate of the exchange reaction compared to the baseline condition without a dopant addition. The results showed better suppression of the exchange reaction using $SrSO_4$ and SeS_2 dopant additions at lower concentration of 0.5 wt.% with similar effect. Also, it was found that a dopant concentration of greater than 1.0 wt.% did not further influence the exchange reaction.

4. ELECTROCHEMICAL METHOD

To prevent the exchange reaction between the liquid flux and the molten steel, an electrical potential was utilized as a preventive measure. The underlying concept was to create a physical barrier between the two regions, effectively hindering the occurrence of the reaction. The objective of this experimental approach was to assess the efficiency of electromotive force in suppressing the aluminum/silica exchange reaction. A range of electrical potentials, varying from 0 to 3 volts (V), was applied based on preliminary calculations and simulation, applying negative force "-" through the molten steel and positive "+" through the molten flux. The oxidation-reduction reactions, which occur during the exchange reaction are shown below,

$$4\ Al^{0} + 3\ Si^{+4}O_2^{-2} = 3\ Si^{0} + 2\ Al^{+3}O_3^{-2} \quad (14)$$

$$\text{Oxidation: } Al^{0} - 3\ e = Al^{3+} \quad (15)$$

$$\text{Reduction: } Si + 4\ e = Si^{0} \quad (16)$$

Through an investigation of the impact of electromotive force exerted on the molten steel and flux, the aim was to gain insights into its potential as a means of controlling and mitigating the undesired reaction at the interface between the steel and slag. The outcomes obtained from these laboratory tests furnish valuable knowledge for advancing the understanding of suppressing the aluminum/silica exchange reaction.

4.1 MATERIALS AND METHODS

The experimental study utilized steel and mold flux with identical compositions, following the slag dopants method outlined in Table 3.1 and Table 3.2. The initial stage of the procedure involved the preparation of a mold flux encapsulated steel sample to prevent additional oxidation during testing. This process entailed melting 30-40 g of flux in a graphite crucible at a temperature of 1300 ℃. Simultaneously, the steel sample weighing 80 g was preheated and subsequently placed into the graphite crucible containing the molten flux after 5-6 minutes in the furnace. Subsequently, the steel sample, along with the encapsulating glass, was transferred to a furnace maintained at 575℃ and gradually cooled until it reached room temperature. Figure 4.1 illustrates the polished and glass encapsulated steel samples.

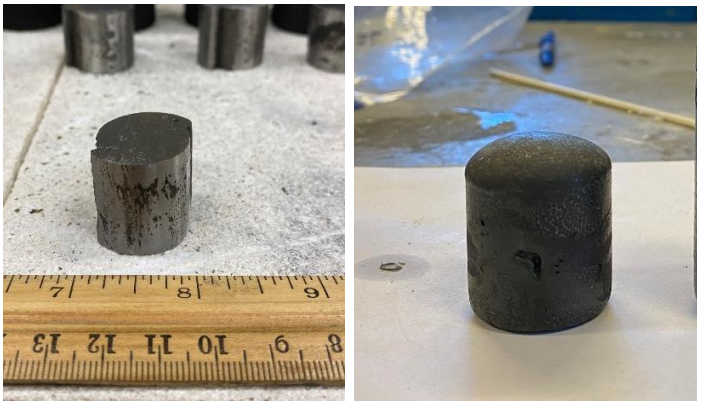

(a) (b)

Figure 4.1 The Polished (a) and Glass Encapsulated (b) Steel Samples.

The making of the top and bottom electrodes for interaction with the molten flux involved the utilization of various materials and specific techniques. To create the top

electrode, a graphite rod and lid were employed, with the lid (diameter of 35 mm) being modified by drilling a 6 mm hole in diameter. This hole was designed to accommodate a graphite rod, which was secured by threading it into the lid.

For the bottom electrode, zirconium diboride (ZrB_2) and steel rod were chosen due to their favorable performance in high-temperature environments. A solid ZrB_2 rod with a diameter ranging from 1.2 to 1.4 mm was inserted into an MgO tube, which had an outer diameter (OD) of 2 mm. The ZrB_2 rod was then connected to a platinum wire, which had a diameter of 1 mm. To protect the platinum wire from the elevated temperatures, it was placed inside an alumina tube.

The resulting electrode configuration can be observed in Figure 4.2, depicting the top electrode composed of a graphite rod and lid, the ZrB_2 rod connected to the platinum wire, and the steel rod utilized in the experiments.

(a) (b) (c)

Figure 4.2 Pictures of Graphite (a), ZrB_2 (b) and Steel (c) Electrodes Used in Experiments.

The experimental trials and subsequent tests employed an induction furnace equipped with a copper coil. The power supply used had voltage and current ranges of 20 V and 30 A respectively, and 6000 watts in power. Data capturing was conducted at regular intervals of 0.5 seconds using a data logger and B-type thermocouple which was put on the bottom of graphite crucible during the test. The copper coil utilized in the setup had an outer diameter (OD) of 90 mm and was made from a copper tube with an outer diameter of 6.25 mm. A visual representation of the materials can be found in Figure 4.3.

(a) (b) (c)

Figure 4.3. Pictures of Induction Furnace with Copper Coil (a), Power Supply (b) and Data Logger (c) Used in Experiments.

4.2 EXPERIMENTAL SETUP

The experimental setup employed an induction furnace, as depicted in Figure 4.3, comprising various components such as a graphite crucible, a MgO crucible, glass, and a steel sample. The graphite crucible possessed dimensions of 62 mm outer diameter (OD), 47 mm inner diameter (ID), and 88 mm height. The high-density MgO crucibles featured an internal diameter of 38 mm and a height of 60 mm. The masses of the steel and glass samples were approximately 80 g and 30-40 g, respectively, maintaining the same steel-to-slag ratio as the slag dopants method. The arrangement of the experimental

configuration within the furnace, including two different bottom electrodes, can be observed in Figure 4.4 and Figure 4.5.

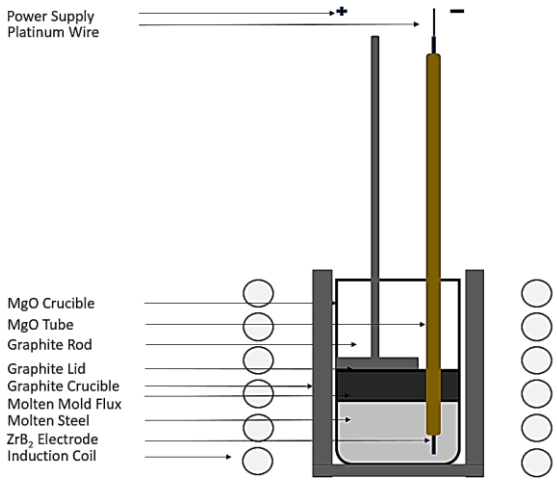

Figure 4.4 Experimental Configuration of Using the ZrB_2 Material as a Bottom Electrode.

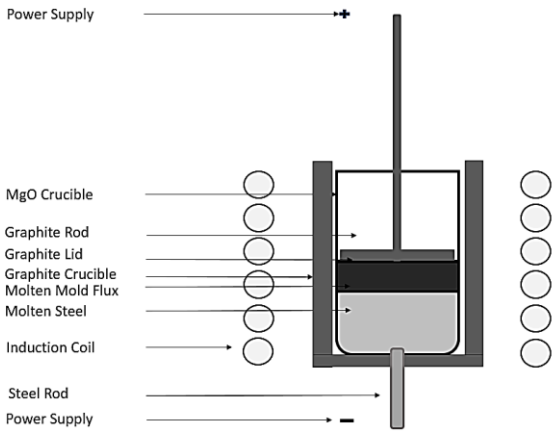

Figure 4.5. Experimental Configuration of Using the Steel Rod as a Bottom Electrode.

For the experiments involving a steel rod as a bottom electrode, a ceramic cylinder was employed as a protective measure. This ceramic cylinder was filled with magnesia dry

vibe material, which served the purpose of safeguarding the thermocouple and the surrounding environment of the furnace against any potential leakage of the liquid steel. Prior to each experiment, alumina tube with the thermocouple inside and the steel rod, were placed inside the ceramic cylinder. After the completion of each test, only the steel rod was replaced while the thermocouple and alumina tube remained unchanged. A visual depiction of the experimental setup before conducting the test is presented in Figure 4.6.

Figure 4.6 Experimental Setup with Ceramic Cylinder Filled with MgO Dry Vibe.

4.3 DETERMINATION OF THE MELTING POINT OF STEEL

To ensure the experimental accuracy, it was imperative to determine the melting point of the steel, which signifies the temperature at which the sample completely transitions into a liquid state within an induction furnace.

For this purpose, a 300 mm long alumina rod was securely attached to the steel sample in advance and positioned inside an MgO crucible located within the induction coil. The furnace was then gradually heated to 1600℃ at a heating rate of 35℃/minute. The thermocouple was positioned as closely as possible to the steel sample, adjacent to the wall of the graphite crucible. Regular evaluations of the steel sample's state of aggregation were

carried out by inserting an alumina rod through an opening in the setup. Consequently, the melting temperature for an 80 g steel sample was determined as 1530℃. Additionally, a JMatPro simulation was conducted to predict the melting temperature of the steel sample, yielding a similar result of approximately 1528℃. This temperature was utilized in the future experiments as a melting point for the steel. The experimental setup is depicted in Figure 4.7.

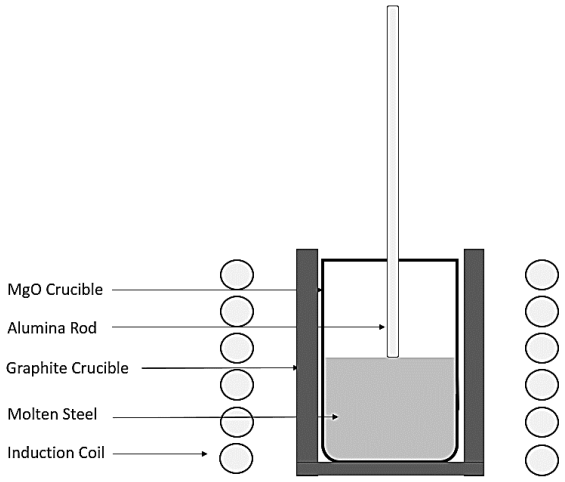

Figure 4.7 The Arrangement of the Alumina Rod During the Melting Point Determination.

4.4 VOLTAGE SWEEP TEST

In order to analyze the relationship between voltage and current in the system and anticipate the average current at specific voltage levels during practical experiments, a series of voltage sweep tests were conducted. These tests involved the utilization of a laptop, a power supply, and an Arduino Project kit, with special code written in the C++ programming language. The experimental arrangement can be observed in Figure 4.8.

(a) (b)

Figure 4.8 Picture Showing the Whole Setup Before the Trial (a) and Close View of the Connection of UNO R3 Controller Board to the Breadboard and Power Supply (b).

A software algorithm was developed to perform a systematic incremental variation of voltage output using a designated button on the Arduino breadboard. The program initiated at a voltage level of 0 V and kept it at 1 V while the system was being heated up to a temperature of 1530°C. Upon complete melting of the steel, the voltage abruptly dropped to 0 V and subsequently ramped up at a rate of 0.025 V per second until reaching 3 V within a time span of 2 minutes. Following this, the voltage was reduced back to 1 V while the system underwent the cooling process, ultimately reaching 0 V once again at the conclusion of the experiment.

To obtain accurate voltage measurements during the experiment, an RC (Resistor-Capacitor) filter configuration was employed. The filter consisted of a 10 Ohm resistor and a 10-mF capacitor, specifically chosen for this purpose. Furthermore, adjustments were made to the code after conducting multiple trials, aiming to generate a more precise voltage signal for the power supply. Figure 4.9 illustrates the voltage outputs obtained both with and without the implementation of the RC filter.

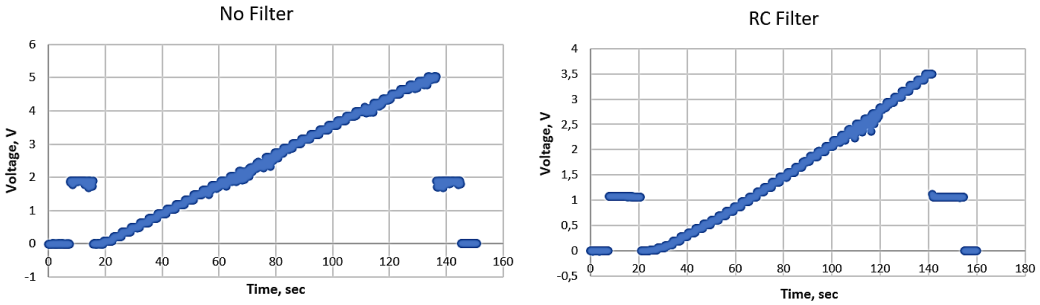

(a) (b)

Figure 4.9. Plots Representing the Voltage Outputs Obtained Both (a) with and (b) without the Implementation of RC Filter.

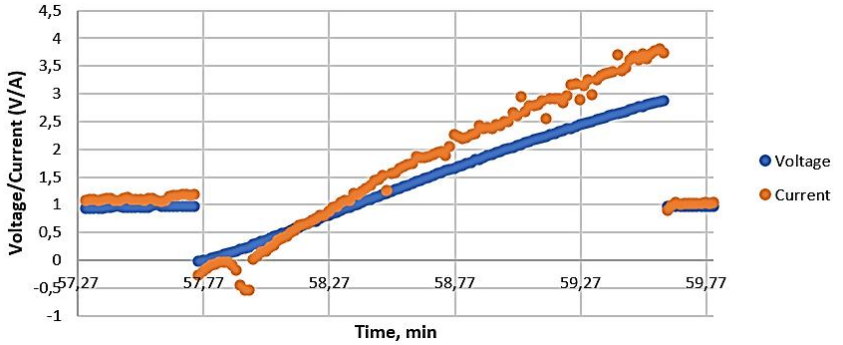

(a)

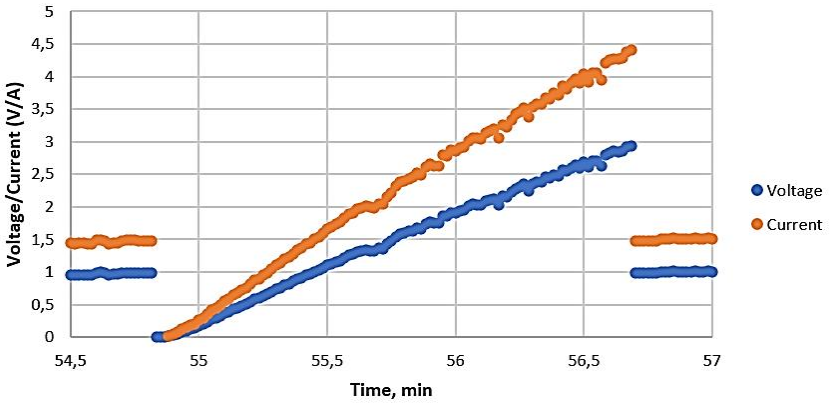

(b)

Figure 4.10 The Outcomes of Both (a) the Exclusive Flux Voltage Sweep at 1300℃ and (b) the Voltage Sweep Conducted on the Steel with Mold Flux at 1530℃.

In order to further investigate the electrical behavior within the mold flux and validate that the measurements of flux resistance were not conducted during the tests with electrochemical suppression, a voltage sweep was exclusively performed in the molten flux at 1300 ℃. The outcomes of both the exclusive flux voltage sweep and the voltage sweep conducted on the steel with mold flux at 1530 ℃ are depicted in Figure 4.10.

The results indicate that the molten steel exhibits greater electrical conductivity compared to the molten flux alone, resulting in higher current values for the same applied voltage within the range of 0 to 3 V.

4.5 CALCULATION OF THE ELECTRICAL POTENTIAL

To estimate the required electrical potential for inhibiting the aluminum/silica exchange reaction, the researchers employed FactSage simulation and conducted calculations based on the chemical potentials of individual species in both steel and mold flux. They utilized a fundamental equation to calculate the free Gibbs energy, considering the number of electrons participating in the reaction and Faraday's constant. These calculations aimed to predict the approximate electrical potential necessary to suppress the mentioned reaction in Equation (1).

$$\Delta G = -nFE \Rightarrow E = \Delta G/(-nF), [V] \quad (17)$$

$$\Delta G = (\sum G_{products} - \sum G_{reactants}), [J/mole] \quad (18)$$

where, n is the number of electrons involved in reaction, (n=12); F is Faraday's constant, F = 96500 C/mole; and E is the electrical potential.

4.5.1 Converting Mass to Moles. Each species of steel sample weighing 80 g and mold flux weighing 30 g were converted into their respective moles. The conversion of the species of steel sample to moles is presented in Table 4.1, while the conversion of the species of mold flux to moles is shown in Table 4.2:

Table 4.1 The Number of Moles of Each Species in the Steel Sample.

Element	Amount in steel, wt.%	Amount in steel, g	Mass converted to moles, mol.
Al	2.84	2.28	0.084
Si	0.48	0.384	0.014
C	0.12	0.08	0.007
Fe	Bal.	77.256	1.383

Table 4.2 The Number of Moles of Each Species in the Mold Flux.

Compound	Amount in flux, wt.%	Amount in flux, g	Mass converted to moles, mol.
SiO_2	37.46	11.238	0.187
CaO	35.17	10.551	0.188
MgO	3.45	1.035	0.026
Al_2O_3	4.68	1.404	0.014
TiO_2	0.18	0.054	0.0007
Fe_2O_3	0.27	0.081	0.0005
MnO_2	0.06	0.018	0.0002

Table 4.2 The Number of Moles of Each Species in the Mold Flux (cont.).

Compound	Amount in flux, wt.%	Amount in flux, g	Mass converted to moles, mol.
P_2O_5	0.03	0.009	0.00006
Na_2O	9.88	2.964	0.048
K_2O	0.11	0.033	0.00035
F	11.26	3.378	0.178
SrO	0.03	0.09	0.0001
ZrO_2	0.03	0.09	0.0007

4.5.2 Determining Limiting Reactant. Limiting reactant has lower quantity per coefficient ratio among reacting species. Aluminum has 4 molecules and 0.084 moles which gives 0.084/4 = 0.021 ratio; silica at the same time has the ratio of 0.187/3 = 0.062. Therefore, it can be stated that aluminum is a limiting reactant in the given reaction.

4.5.3. Stoichiometry of Reaction. It's given that aluminum has weight of 2.28 g, which is 0.084 mol, therefore moles of each species can be calculated based on the exchange reaction (Equation 1)

0.084 mol. Al x (3 mol. SiO_2/4 mol. Al) = 0.063 mole SiO_2.

0.084 mol. Al x (2 mol. Al_2O_3/4 mol. Al) = 0.042 mole Al_2O_3.

0.084 mol. Al x (3 mol. Si/4 mol. Al) = 0.063 mole Si.

4.5.4. FactSage Simulation and Calculation of Change in Free Gibbs Energy. Equilib mode and FACTPS, FSStel, FTmisc, FToxid data sets were utilized to determine free Gibbs energy of each species of the system. To calculate free Gibbs energy and chemical potentials, the following Equation 8 and Equation 9 were utilized.

$$\Delta G = (\sum \mu_{\text{products}} - \sum \mu_{\text{reactants}}) \quad (19)$$

$$\mu = \mu_i^0 + RT \ln a_i \quad (20)$$

Figure 4.11 and Figure 4.12 display the parameters provided as inputs in the FactSage software, enabling the determination of the activities of each species present in the molten steel and mold flux. Specifically, Figure 4.13 exhibits the activity values of A and Si within the molten steel, while Figure 4.14 showcases the activity values of Al_2O_3 and SiO_2 within the mold flux.

```
0.084 Al  +  0.014 Si  +  0.007 C  +  1.383 Fe  =
(1530,1,liq-FSstel,#1) (1530,1,liq-FSstel,#1) (1530,1,liq-FSstel,#1) (1530,1
```

Figure 4.11 Input Parameters for the Steel Sample.

```
0.187 SiO2  +  0.188 CaO  +  0.026 MgO  +  0.014 Al2O3  +
(1530,1,liq-FToxid,#1) (1530,1,liq-FToxid,#1) (1530,1,liq-FToxid,#1) (1530,1
0.0007 TiO2  +  0.0005 Fe2O3  +  0.0002 MnO2  +  0.00006 P2O5  +
(1530,1,liq-FToxid,#1) (1530,1,sl-FToxid,#1) (1530,1,s-FToxid,#1) (1530,1,li
0.048 Na2O  +  0.00035 K2O  +  0.178 F  +  0.0001 SrO  +
(1530,1,liq-FToxid,#1) (1530,1,liq-FToxid,#1) (1530,1,g-FactPS,#1) (1530,1,1
0.0007 ZrO2  =
(1530,1,liq-FToxid,#1)
```

Figure 4.12 Input Parameters for the Mold Flux.

PHASE: LIQUID#1(;#2)	mol	MOLE FRACTION	ACTIVITY
Al	8.4000E-02	8.6286E-02	2.1102E-03
C	7.0000E-03	7.1905E-03	1.6621E-05
Fe	8.6851E-01	8.9214E-01	8.4590E-01
Si	1.4000E-02	1.4381E-02	6.2540E-06
TOTAL:	9.7351E-01	1.0000E+00	1.0000E+00

Figure 4.13 Activities of Al and Si in Molten Steel.

PHASE: Slag-liq#1(;#2)	mol	MOLE FRACTION	ACTIVITY
Na2O	3.4534E-02	7.3227E-02	5.5107E-09
K2O	2.6596E-04	5.6396E-04	1.9307E-15
Al2O3	5.2992E-03	1.1237E-02	2.6271E-05
SiO2	1.6265E-01	3.4488E-01	8.9129E-02

Figure 4.14. Activities of Al_2O_3 and SiO_2 within the Mold Flux.

To calculate chemical potential of each species in solutions, the standard chemical potentials μ_0 from literature were utilized [26].

$$\mu^0_{Al} = 0 \text{ J/mol}$$

$$\mu^0_{Si} = 0 \text{ J/mol}$$

$$\mu^0_{SiO2} = -856670 \text{ J/mol}$$

$$\mu^0_{Al2O3} = -1582390 \text{ J/mol}$$

$\mu_{Al} = \mu_{Al}^0 + RT \ln a_{Al} = 0$ J/mol + 8.314 J/mol x 1803 K x ln (2.11×10^{-3}) = -9.24×10^4 J/mol

$\mu_{Si} = \mu_{Si}^0 + RT \ln a_{Si} = 0$ J/mol + 8.314 J/mol x 1803 K x ln (6.25×10^{-6}) = -1.8 x10^5 J/mol

$\mu_{Al2O3} = \mu_{Al2O3}^0 + RT \ln a_{Al2O3} = -1582390$ J/mol + 8.314 J/mol x 1803 K x ln (2.63×10^{-5}) = -1.74 x 10^6 J/mol

$\mu_{SiO2} = \mu_{SiO2}^0 + RT \ln a_{SiO2} = -856670$ J/mol + 8.314 J/mol x 1803 K x ln (8.9×10^{-2}) = -8.93 x 10^5 J/mol

$\Delta G = (\sum \mu_{products} - \sum \mu_{reactants}) = (-3 \times 1.8 \times 10^5$ J/mol – 2 x 1.74 x 10^6 J/mol) – (- 4 x 9.24 x 10^4 J/mol – 3 x 8.93 x 10^5 J/mol) = -9.72 x 10^5 J/mol

$E = \Delta G/-nF = -9.72 \times 10^5/-(12 \times 96500) = 0.839$ V.

The findings indicate that an electrical potential of approximately 0.84 V is required to inhibit the aluminum/silica exchange reaction between the molten steel and mold flux. Further testing will be conducted to validate this observation.

4.6 EXPERIMENTAL PROCEDURE

The experiment involved placing a graphite crucible with an MgO crucible and an encapsulated steel sample inside an induction coil. A graphite rod was positioned on top of the cold flux, and a ZrB_2 electrode (enclosed in an MgO tube) was placed at the bottom of the MgO crucible. The entire system was covered with insulation material. The Pt wire, already in contact with the ZrB_2 electrode, was connected to the "-" terminal of the power supply, while the graphite rod was connected to the "+" terminal.

The induction furnace was turned on, and the heating of the induction coil commenced at a rate of 35°C per minute. A data logger was initiated to record voltage,

current, and temperature readings every second. Once the flux reached a molten state at 1300°C, the positioning of the graphite rod on top of the molten flux was checked, and the electric potential was applied.

When the temperature reached 1530°C, indicating the steel had melted, a timer was started and set for 5 minutes. Subsequently, the induction furnace was switched off, but the application of voltage continued until the steel was about to solidify. At that point, all electrodes were removed, and the sample was quenched in the water.

The identical methodology was utilized with a steel rod as the bottom electrode. However, rather than rapidly cooling the sample, it underwent a controlled cooling process in air until reaching a temperature of 1000-1100℃, after which it was extracted from the experimental system.

4.7 RESULTS AND DISCUSSION

The initial experimental approach involved utilizing ZrB_2 ceramic material as the bottom electrode. However, the results of the trials demonstrated that the ZrB_2 electrode exhibited poor conductivity at high temperatures, specifically around 1530℃. The exposed portion of the material in contact with the molten steel experienced consistent degradation, making it unsuitable for reuse in subsequent trials due to its brittle nature. Furthermore, the ZrB_2 electrode was susceptible to breakage during the cleaning process to remove oxides, making it a time-consuming and delicate procedure. Additionally, the connection between the ZrB_2 electrode and the Pt wire proved to be unreliable during testing, as the portion of the wire wrapped around the electrode consistently weakened at elevated temperatures.

Furthermore, it was consistently observed that the MgO tube experienced erosion by the molten flux at the slag level, leading to the exposure of the ZrB_2 electrode to the slag. Consequently, this exposure resulted in the disruption of the electrical circuit. Figure 4.15 provides visual representation of the ZrB_2 electrode before and after the experiment, contained within the MgO tube.

(a) (b)

Figure 4.15 ZrB_2 Electrode (a) Before and (b) After the Experiment, Contained within the MgO Tube.

Subsequently, following multiple experimental attempts, a decision was made to modify the configuration by employing a steel rod as the bottom electrode. As previously explained, a dry vibe of MgO was utilized to fill the ceramic cylinder and the gaps between the graphite and MgO crucibles. This measure aimed to safeguard the system against potential leakage of steel or slag. Notably, no cases of steel or flux leakage were observed, and the walls of the MgO crucible remained with no cracks. Upon completion of the tests, the steel sample remained within the MgO crucible. Throughout the duration of the tests, the graphite electrodes exclusively contacted the flux, resulting in the almost clean condition of the electrode bottoms. A visual representation of the steel rod within the MgO

crucible, the graphite electrode, the steel sample, and the slag after the test is presented in Figure 4.16.

(a) (b) (c) (d)

Figure 4.16 Picture of (a) Steel Rod within the MgO Crucible, (b) Graphite Electrode, (c) Steel Sample, and (d) Slag After the Test.

The experimental setup involved the application of different electrical potentials ranging from 0 to 3 V across the steel/slag system utilizing ZrB_2 and steel as bottom electrodes. To better understand the voltage/current change during the experiment, there was a data logger capturing the current, voltage and temperature in the system. One of the plots is shown in Figure 4.17 which was captured during the test with 0.84 V.

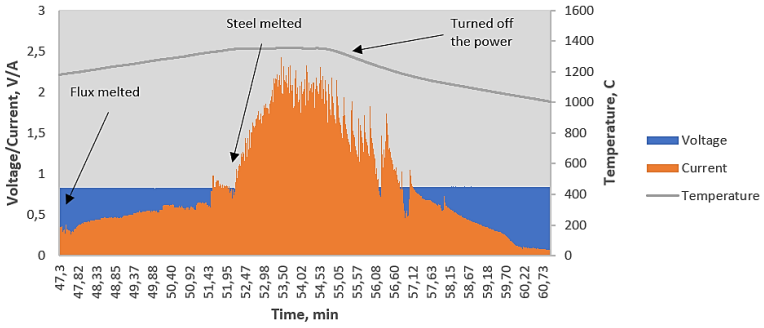

Figure 4.17 Voltage/Current and Temperature Profiles During the Test of 0.84 V Applied.

Based on the provided graph, it was observed that the electrical conductivity of the molten flux was significantly lower than that of the molten steel. This discrepancy proved advantageous in our experimental setup as it served as an additional confirmation of the steel's melting point when there was a sudden increase in the electrical current within the system.

Subsequently, OES and XRF analysis were conducted to assess the efficiency of mitigating the exchange reaction. The outcomes of the OES analysis on the steel samples are depicted in Figure 4.18 and Figure 4.19, while additional XRF results can be found in the Figure 4.20 and Figure 4.21.

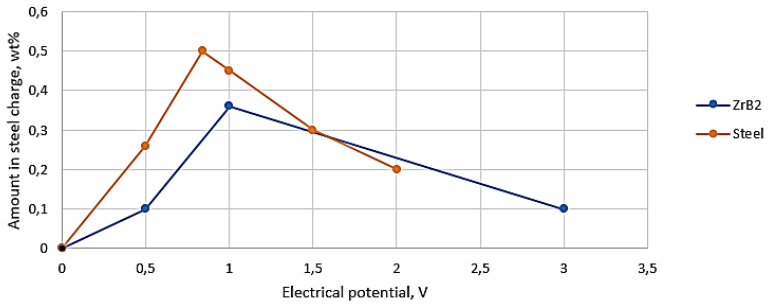

Figure 4.18. The Al Content in Steel Measured by OES.

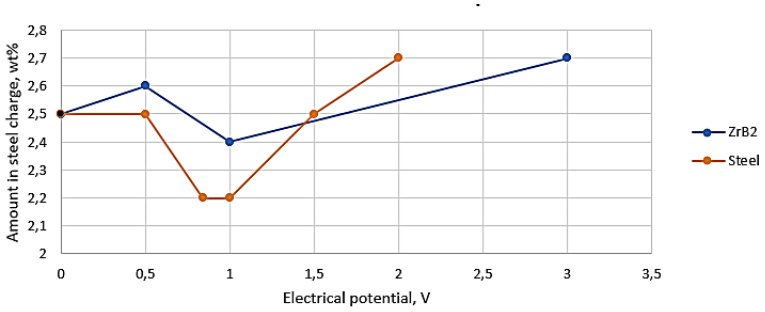

Figure 4.19. The Si Content in Steel Measured by OES.

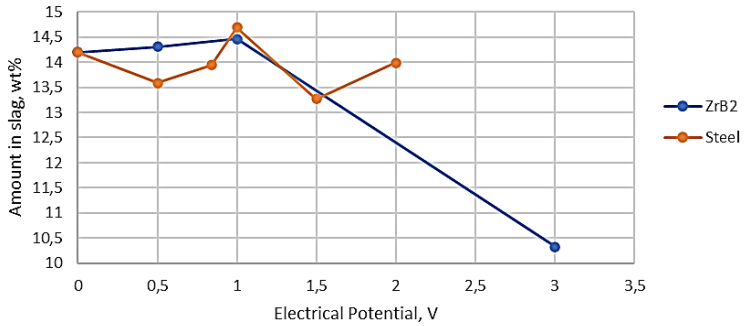

Figure 4.20 The Al_2O_3 Content in Slag Measured by XRF.

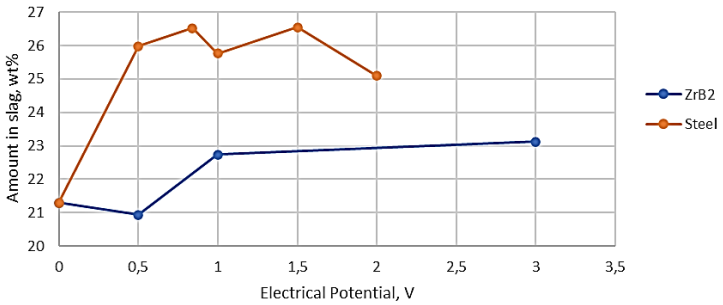

Figure 4.21 The SiO_2 Content in Slag Measured by XRF.

Significant inhibition of the exchange reaction was not observed when the electrical voltage deviated from 0.84 V in either direction in comparison to the baseline, as observed in both methods. Conversely, electrical potentials of 0.84 and 1.0 volts exhibited enhanced suppression of the exchange reaction, leading to increased aluminum content and decreased silicon content in the steel compared to the baseline. Mass balance calculations show almost similar results as it was with slag dopants method giving the total Al reacted with air of around 50 percent. The overall Al and Si content change with the applied voltage is illustrated in Table 4.3. The reason why higher electrical voltage is not as effective is still

unknown. Other reactions may be activated when higher electrical voltage is applied. Further investigations are required to clarify the cause.

Table 4.3 OES Analysis of All Experiments within the Time Frame of 5 Minutes.

Applied voltage, V	Al in teel, wt.%	Si in steel, wt.%	Type of electrode
0	0	2.5	Baseline
0.5	0.1	2.6	ZrB_2 electrode
0.5	0.26	2.5	Steel Rod
0.84	0.5	2.2	Steel Rod
1.0	0.36	2.4	ZrB_2 electrode
1.0	0.45	2.2	Steel Rod
1.5	0.3	2.5	Steel Rod
2.0	0.2	2.7	Steel Rod
3.0	0.1	2.7	ZrB_2 electrode

This effect was also evident in the XRF results, particularly in tests where a steel rod was utilized as the bottom electrode. Some of the slag analyses deviated from the OES results, particularly in experiments involving ZrB_2 as an electrode, which can be attributed to the imperfect nature of most experiments conducted with this electrode. Moreover, it is important to highlight that the inhibition of the reaction becomes evident once the steel and slag have solidified. This outcome demonstrates highly encouraging findings when compared to the first method of adding dopants, where samples were rapidly cooled without allowing for solidification in air.

4.8 SUMMARY

To investigate the aluminum/silica exchange reaction between steel and mold flux, a study to examine the impact of applied electrical potential on the reaction in the context of continuous casting was conducted. Through thermodynamic analysis, it was determined that an electrical voltage of 0.84 V is required to suppress the reaction for the specific steel grade under investigation. Subsequently, electrical potentials ranging from 0.5 to 3.0 volts were applied within the system consisting of molten high aluminum steel and flux at a temperature of 1530 ℃ using an induction furnace with two different materials used as a bottom electrode.

The experimental results demonstrated that the application of electrical potentials effectively slowed down the rate of the exchange reaction, bringing it closer to the thermodynamically predicted value of 0.84 volts, especially using steel rod. These findings contribute valuable insights into the mitigation of the reaction between steel and mold flux during industrial processes.

5. CONCLUSION

In conclusion, this study investigated the impact of slag dopants and applied electrical potential on the aluminum/silica exchange reaction between steel and mold flux in the context of continuous casting. The results showed that all dopants tested, including $CaSO_4$, $SrSO_4$, and SeS_2, at concentrations of 0.5 wt.%, 1.0 wt.%, and 2.5 wt.%, slowed down the exchange reaction compared to the baseline condition without dopant addition. Among the dopants, $SrSO_4$ and SeS_2 at a concentration of 0.5 wt.% demonstrated slightly better suppression of the reaction, resulting in higher Al content and lower Si content in the steel. The dopant concentration above 1.0 wt.% did not further influence the exchange reaction.

Additionally, the application of electrical potentials showed promising results in inhibiting the exchange reaction. Voltages of 0.84 and 1.0 V were found to be effective in suppressing the reaction, leading to increased Al content and decreased Si content in the steel compared to the baseline condition.

The use of different electrode materials, including ZrB_2 and steel, was explored in the experimental setup. However, the ZrB_2 electrode exhibited poor conductivity and was prone to degradation, making it unsuitable for reuse. The steel rod electrode proved to be more reliable compared to ZrB_2 material. Additionally, the electrical conductivity of the molten flux was found to be significantly lower than that of the molten steel, providing additional confirmation of the steel's melting point during the experiment.

The OES and XRF analysis confirmed the efficiency of both the slag dopants and applied electrical potential in mitigating the exchange reaction. Mass balance calculations

indicated that around 50% of the aluminum reacted with air instead of the flux in all experiments.

Overall, the findings suggest that both slag dopants and applied electrical potential can effectively suppress the aluminum/silica exchange reaction. The results provide valuable insights for optimizing the continuous casting process and improving the quality of steel production. Further research could focus on reducing the dopant concentrations and trying to apply electrical potential in range between 0.84 and 1.0 volts or combine both methods with the best dopant addition and electrical voltage to achieve even better suppression of the exchange reaction. Other possible reactions between mold flux and molten steel are not explored in this study. Hence, further investigations on possible exchange reactions due to dopant additions and applied electrical voltages are also required.

BIBLIOGRAPHY

[1] G. Bezuidenhout and G. Pistorius, “Effect of Alumina Pickup on Mold Flux Viscosity in Continuous Slab Casting”. Ironmaking & Steelmaking Vol 27. (2000) 387-391. 10.1179/030192300677705.

[2] MIT Report: On the Road in 2035, 2008. http://web.mit.edu/sloan-auto-lab/research/beforeh2/otr2035/.

[3] Huixiang Yu, Dexin Yang, Jiaming Zhang, Guangyuan Qiu, and Ni Zhang, Effect of Al content on the reaction between Fe−10Mn−xAl (x = 0.035wt%, 0.5wt%, 1wt%, and 2wt%) steel and CaO−SiO2−Al2O3−MgO slag, Int. J. Miner. Metall. Mater., 29(2022), No. 2, pp. 256-262. https://doi.org/10.1007/s12613-021-2298-y.

[4] Mills, K., & Fox, A. (2002). Metals, Slags, Glasses: High Temperature Properties & Phenomena. Mould Fluxes, Mills Symposium, The Institute of Materials, 121-132.

[5] Thomas, B. (2001). Modeling of the Continuous Casting of Steel- Past, Present and Future. Electric Furnace Conf. Proc. ISS, 59, 3-30.

[6] S. Seetharaman, A. McLean, R. Guthrie and S. Sridhar, Treatise on Process Metallurgy.

[7] https://www.ispatguru.com/inclusions-in-continuous-cast-steel-and-theirdetection. Inclusions in Continuous Cast Steel, May 2023.

[8] E. Brandaleze, G. Di Gresia, L. Santini, A. Martín and E. Benavidez, Mold Fluxes in the Steel Continuous Casting Process, Chapter 7, http://dx.doi.org/10.5772/50874.

[9] M.-A. Van Ende, I.-H. Jung, Development of a Thermodynamic Database for Mold Flux and Application to the Continuous Casting Process. Cutting Edge of Computer Simulation of Solidification, Casting and Refining, 2014. DOI: http://dx.doi.org/10.2355/isijinternational.54.489.

[10] T. Wu, S. He, L. Zhu and Q. Wang, Study on Reaction Performances and Applications of Mold Flux for High-Aluminum Steel, 2015. Materials Transactions, Vol. 57, No. 1 (2016) pp. 58 to 63.

[11] S. Street, K. James, N. Minor, A. Roelant, and J. Tremp: Iron Steel Technol., 2008, vol. 5, pp. 38–49.

[12] J.W. Cho, K. Blazek, M. Frazee, and Hongbin. Yin: ISIJ Int., 2013, vol. 53 (1), pp. 62–70.

[13] K. Blazek, H. Yin, G. Skoczylas, M. McClymonds, and M. Frazee: Iron Steel Technol., 2011, vol. 8 (3), pp. 231–40.

[14] J. Yang, H. Cui, J. Zhang, O. Ostrovski, C. Zhang, and D. Cai: Interfacial Reaction Between High-Al Steel and CaO-Al2O3-Based Mold Fluxes with Different CaO/Al2O3 Ratios at 1773 K (1500C). The Minerals, Metals & Materials Society and ASM International 2019. https://doi.org/10.1007/s11663-019-01667-0.

[15] S.-Y. Song, J. Li, and W. Yan: Reaction between molten steel and CaO-SiO2-MgO-Al2O3-Fe_tO slag under varying amounts of converter carryover slag. Journal of Materials Science and Technology, Vol. 17, 2022. https://doi.org/10.1016/j.jmrt.2022.01.154.

[16] Y.-B. Kang, M.-S. Kim, S.-W. Lee, J.-W. Cho, M.-S. Park, H.-G. Lee: A Reaction Between High Mn-High Al Steel and CaO-SiO2-Type Molten Mold Flux: Part II. Reaction Mechanism, Interface Morphology, and Al2O3 Accumulation in Molten Mold Flux. Metallurgical and Materials Transactions, 2012. https://www.researchgate.net/publication/257709025.

[17] M.-S. Kim, S.-W. Lee, J.-W. Cho, M.-S. Park, H.-G. Lee, and Y.-B. Kang: A Reaction Between High Mn-High Al Steel and CaO-SiO2-Type Molten Mold Flux: Part I. Composition Evolution in Molten Mold Flux. The Minerals, Metals & Materials Society and ASM International 2012. DOI: 10.1007/s11663-012-9770-z.

[18] M.-S. Kim, Y.-B. Kang: Development of a multicomponent reaction rate model coupling thermodynamics and kinetics for reaction between high Mn-high Al steel and CaO-SiO2-type molten mold flux. Calphad 2018. https://doi.org/10.1016/j.calphad.2018.02.010.

[19] S. He, Q. Wang, J. Zeng, M. Zhang, and B. Xie: J. Iron. Steel Res. Int., 2009, vol. 21, pp. 59–62.

[20] K. Blazek, H. Yin, G. Skoczylas, M. McClymonds, and M.Frazee: Iron Steel Technol., 2011, vol. 8 (3), pp. 231–40.

[21] Q. Wang, S.T. Qiu, and P. Zhao: Metall. Mater. Trans. B, 2012, vol. 43B, pp. 424–30.

[22] B. Ozturk, and E.T. Turkdogan: Met. Sci., 1984, vol. 18, pp. 306–310.

[23] Kawasaki Steel Joint-Stock Company: Japanese Patent, No.57-184563. 1982-11-13.

[24] M.-S. Kim, and Y.-B. Kang: A Reaction Model to Simulate Composition Change of Mold Flux During Continuous Casting of High Al Steel. TMS (The Minerals, Metals & Materials Society), 2016. Advances in Molten Slags, Fluxes, and Salts: Proceedings of The 10th International Conference on Molten Slags, Fluxes and Salts (MOLTEN16).

[25] T. Wysong. Mold Flux Reaction Suppression, 2020. PowerPoint Presentation for PSMRC Meeting.

[26] D. R. Stull and H. Prophet: "`JANAF Thermochemical Tables"' Natur. Bur. Stand (U.S.) 1971.

VITA

Kuanysh Nurbekuly Yermukhanbetov, was born in Oskemen, Kazakhstan. In September 2011 Kuanysh started his undergraduate degree in metallurgical engineering at East Kazakhstan State Technical University. Once he graduated, he started working at Kazzinc Ltd. as a plant metallurgist and then as a shift supervisor. At the same time, he was pursuing his master's degree in engineering and technology at East Kazakhstan State Technical University. In 2017 he started his career as a Technical Sales Engineer at Quantum Group and ASCOR Production Association, he worked there for 2 years, and while working he earned a bachelor's degree in economics and business at East Kazakhstan State University named after S. Amanzholov.

Kuanysh began his graduate work at Missouri University of Science and Technology August 2021 as a master's student in Metallurgical Engineering at Materials Science and Engineering Department. He took part and continued one of the senior design projects and had funding for his research from the Kent D. Peaslee Steel Manufacturing Research Center (PSMRC) and Fulbright Foreign Student Program. His research was focused on suppressing the aluminum/silica exchange reaction between steel and mold flux. Kuanysh had the chance to collaborate with numerous colleagues in the steel industry and had the privilege of visiting various plants for tours. Throughout his master's program, Kuanysh also had the opportunity to engage in research alongside several undergraduate and graduate students. Kuanysh received his M.S. degree in Metallurgical Engineering in July 2023 from Missouri University of Science and Technology.